Raman transport and magnetization study of the $RuSr_2R_{2-x}Ce_xCu_2O_{10+\delta}$ (R=Gd, Eu) high-temperature superconducting cuprates

G. V. M. Williams and M. Ryan
Industrial Research Limited, P.O. Box 31310, Lower Hutt, New Zealand
(Received 4 January 2001; published 13 August 2001)

We present the results from a Raman transport and magnetization study on $RuSr_2R_{2-x}Ce_xCu_2O_{10+\delta}$. This compound has been shown to exhibit the coexistence of superconducting and magnetic order. Unlike the other superconducting ruthenate cuprate, $RuSr_2RCu_2O_8$, $RuSr_2R_{2-x}Ce_xCu_2O_{10+\delta}$ contains a significant ferromagnetic component. We find that the peak in the low-field zero-field-cooled magnetization data increases with increasing Ce concentration. This increase is mirrored by an increase in the saturation magnetization at 9.5 kG. However, there is no direct correlation between these increases and the superconducting transition temperature. Furthermore, there are no well-defined changes in either the resistance or the thermopower data that can be correlated with the magnetic-ordering transition. A simple explanation for the increase in the saturation magnetization at 9.5 kG is that, similar to $SrRuO_3$, the RuO_2 layers in $RuSr_2R_{2-x}Ce_xCu_2O_{10+\delta}$ are itinerant ferromagnetic metals. We show that the $RuSr_2R_{2-x}Ce_xCu_2O_{10+\delta}$ transport data can be interpreted in terms of both the resistance and thermopower being dominated by the CuO_2 layers. In this interpretation, the RuO_2 layers only affect the resistance in the CuO_2 layers via exchange coupling and possible spin scattering. The Raman spectra is essentially the same as that found in $RuSr_2RCu_2O_\delta$ and there is no evidence of Raman modes that can be associated with the $R_{2-x}Ce_xO_2$ substructure.

DOI: 10.1103/PhysRevB.64.094515 PACS number(s): 74.72.−h, 74.25.Fy, 74.25.Ha

INTRODUCTION

It has recently been shown that both $RuSr_2R_{2-x}Ce_xCu_2O_{10+\delta}$ and $RuSr_2RCu_2O_8$ (R=Gd, Eu) display superconducting and magnetic order with the magnetic-ordering temperature being up to four times greater than the superconducting transition temperature.[1,2] These superconductors were discovered by Bauernfeind, Widder, and Braun[3,4] and the unit cells are assumed to be similar to $TaSr_2Nd_{2-x}Ce_xCu_2O_{10+\delta}$,[5] $NbSr_2Eu_{2-x}Ce_xCu_2O_{10+\delta}$, and $NbBa_2RCu_2O_8$.[6] Most research effort has been focused on $RuSr_2RCu_2O_8$ where a number of studies have reported that $RuSr_2RCu_2O_8$ is a ferromagnetic superconductor.[7–14] This generated considerable interest because superconductivity cannot coexist with magnetic order without some form of accommodation, for example, via a spontaneous vortex phase or by a modulation of the respective order parameters.[10] However, a neutron powder-diffraction study showed that the low-field magnetic order in $RuSr_2GdCu_2O_8$ is predominantly antiferromagnetic in the RuO_2 layers and that there is a magnetic reorientation with increasing applied magnetic field.[15] A magnetization study on $RuSr_2EuCu_2O_8$ showed that the magnetization data could be interpreted in terms of predominantly low-field antiferromagnetic order ($0.05\mu_B$/Ru at 5 K) and a spin reorientation to ferromagnetic order with increasing magnetic field.[16] In the case of $RuSr_2GdCu_2O_8$ the remanent magnetization is higher [$0.15\mu_B$/Ru (Ref. 16) or $0.115\mu_B$/Ru (Ref. 17) at 5 K] but is still within the upper estimate of a ferromagnetic component determined from a powder-neutron-diffraction study.[15]

Although, superconducting $RuSr_2R_{2-x}Ce_xCu_2O_{10+\delta}$ has not been studied as extensively as $RuSr_2RCu_2O_8$, it is apparent that it is more interesting because there is evidence that $RuSr_2R_{2-x}Ce_xCu_2O_{10+\delta}$ is a ferromagnet.[1,18,19] The temperature dependence of the magnetization and the saturation magnetization from $RuSr_2R_{2-x}Ce_xCu_2O_{10+\delta}$ (x=0.4,0.6) have been interpreted in terms of localized Ru moments with significant spin canting.[1,18] Furthermore, the data have been interpreted in terms of the coexistence of superconductivity and ferromagnetism where there is a spontaneous vortex phase for temperatures near the superconducting transition temperature.[19]

By comparison with the $NbSr_2Eu_{2-x}Ce_xCu_2O_{10+\delta}$ and $NbBa_2RCu_2O_8$ analogs, it is clear that there should be significant differences in the electronic and magnetic properties of $RuSr_2R_{2-x}Ce_xCu_2O_{10+\delta}$ and $RuSr_2RCu_2O_8$. This is apparent in Fig. 1 where the structures of $RuSr_2R_{2-x}Ce_xCu_2O_{10+\delta}$ and $RuSr_2RCu_2O_8$ are shown (based on the $NbSr_2R_{2-x}Ce_xCu_2O_{10+\delta}$ and $NbBa_2RCu_2O_8$

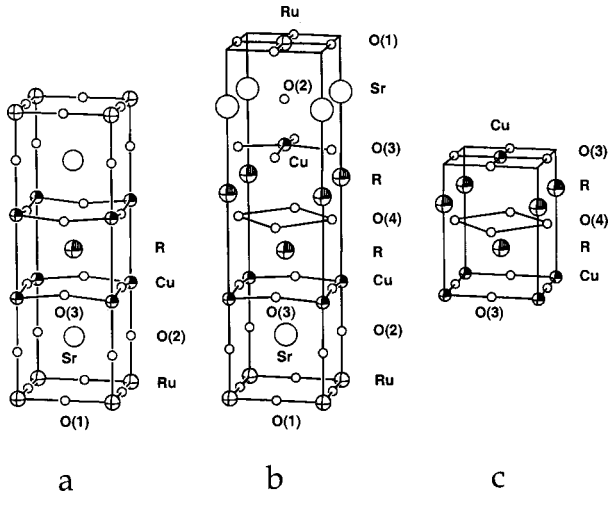

FIG. 1. Structures for (a) $RuSr_2RCu_2O_8$, (b) $RuSr_2R_{2-x}Ce_xCu_2O_{10+\delta}$, and (c) $Nd_{2-x}Ce_xCuO_4$.

analogs[6]). The only significant structural difference between $NbBa_2RCu_2O_8$ and $RuSr_2GdCu_2O_8$ is that the RuO_6 octahedra in $RuSr_2GdCu_2O_8$ are known to be rotated about the *c* axis by ~14° (Refs. 8 and 11) (one study also reported a buckling of the Ru-O-Cu bond[11]). These rotations form coherent domains extending up to ~20 nm. It is not known if the RuO_6 octahedra in $RuSr_2R_{2-x}Ce_xCu_2O_{10+\delta}$ is also rotated. It can be seen in Fig. 1 that $RuSr_2RCu_2O_8$ is essentially a CuO_2 bilayer superconductor. However, $RuSr_2R_{2-x}Ce_xCu_2O_{10+\delta}$ (based on the reported $NbSr_2Eu_{2-x}Ce_xCu_2O_{10+\delta}$ structure) contains an $R_{2-x}Ce_xO_2$ structure in between the CuO_2 layers that is similar to that seen in the $R_{2-x}Ce_xCuO_4$ electron-doped T' structure. The comparison is more evident in Fig. 1(c) where we show the $R_{2-x}Ce_xCuO_4$ T' structure. Thus, the transport and superconductivity behavior in the CuO_2 layers might be expected to be similar to that of the single-CuO_2-layer superconductors. Unlike $RuSr_2GdCu_2O_8$, the Ru atoms in $RuSr_2R_{2-x}Ce_xCu_2O_{10+\delta}$ (based on the reported $NbSr_2Eu_{2-x}Ce_xCu_2O_{10+\delta}$ structure) are not directly above each other in the adjacent RuO_2 layers. It is therefore likely that the Ru-Ru exchange energy in the *c* axis direction is significantly different.

We have performed a Raman transport and magnetization study of $RuSr_2R_{2-x}Ce_xCu_2O_{10+\delta}$ with the aim to understand the vibrational, magnetic, and superconducting behavior of $RuSr_2R_{2-x}Ce_xCu_2O_{10+\delta}$. We show below that the saturation magnetization at 9500 G can be interpreted in terms of itinerant ferromagnetism in the RuO_2 layers. Furthermore, the transport data are dominated by the CuO_2 layers and there is possibly weak coupling between the carriers in the CuO_2 layers and the RuO_2 layers. We also show that the Raman modes are similar to those found in $RuSr_2RCu_2O_8$.

EXPERIMENTAL DETAILS

The $RuSr_2R_{2-x}Ce_xCu_2O_{10+\delta}$ samples were made from a stoichiometric mixture of RuO_2, $Sr(CO_3)_2$, CeO_2, CuO, and Gd_2O_3 or Eu_2O_3. The samples were first annealed in air at 960 °C for 16 h and then (i) heated at 1010 °C in flowing N_2 for 10 h, (ii) heated at 1050 °C in flowing O_2 for 10 h, (iii) heated at 1055 °C in flowing O_2 for 10 h and then (iv) heated at 1060 °C in flowing O_2 for seven days. The samples were then cooled to room temperature at a rate of 4 K/min. The sintering in N_2 gas is required to suppress the $SrRuO_3$ phase.[4] This results in Sr_2RRuO_6, CeO_2, and CuO. A $La_{1.87}Sr_{0.13}CuO_4$ sample was made from a stoichiometric mix of La_2O_3, $Sr(NO_3)_2$, and CuO. The powder was annealed at 700 °C for 1 h and then pressed into pellets, which were heated at 990 °C, 1010 °C, and 1030 °C in air for 48 h.

The samples were characterized and the lattice parameters obtained, using x-ray diffraction (XRD) with a Co K_α x-ray tube. The $La_{1.87}Sr_{0.13}CuO_4$ sample was single phase. There was no evidence of $SrRuO_3$, CeO_2, CuO, $RuSr_2RCu_2O_8$, Gd_2CuO_4, or $Sr_3Ru_2O_7$ in the $RuSr_2R_{2-x}Ce_xCu_2O_{10+\delta}$ XRD patterns after the final 1060 °C synthesis. However, samples with $x \leqslant 0.8$ displayed a small fraction of excess Sr_2GdRuO_6 ($<\sim 7\%$ for $x=0.5$) with the excess Sr_2GdRuO_6 systematically decreasing with increasing Ce concentration. There were also extra weak peaks for $x \leqslant 0.8$ that could not be indexed to the $RuSr_2R_{2-x}Ce_xCu_2O_{10+\delta}$ I4/mmm space group or other possible impurity phases. We show later that the small Sr_2GdRuO_6 impurity fraction did not effect T_c or the magnetization data.

The Raman data were obtained on ceramic-powder samples using the 514.5-nm line of a Ar-ion laser. The incident power was less than 20 mW. The incident light was vertically polarized and the scattered light was unpolarized. However, the polarization sensitivity of the double monochromator and the CCD detector meant that the detected light was predominantly vertically polarized. The resistance data was obtained using the four-terminal technique and the thermopower data was obtained using the standard differential method. The variable-temperature magnetization data were obtained using a vibrating-sample magnetometer for temperatures greater than 15 K and for magnetic fields of up to 10 000 G. One sample was also measured using a SQUID magnetometer.

A part of the $RuSr_2Gd_{1.4}Ce_{0.6}Cu_2O_{10+\delta}$ sample was annealed at 600 °C in 0.1% O_2 and 99.9 % N_2 gas for 14 h. The decrease in δ was estimated from the change in mass to be 0.10 and there was no evidence of superconductivity. Another part of the $RuSr_2Gd_{1.4}Ce_{0.6}Cu_2O_{10+\delta}$ sample was annealed at 100 bars in oxygen for 12 h at 600 °C, ramped to 350 °C over 24 h, and annealed at 350 °C for 72 h. We observed a mass change corresponding to an increase in δ of 0.07.

RESULTS AND ANALYSIS

The $RuSr_2Gd_{2-x}Ce_xCu_2O_{10+\delta}$ lattice parameters were, within experimental error, independent of Ce concentration. We found that $a=(3.840\pm0.004)$ Å and $c=(28.58\pm0.03)$ Å. These values are comparable to those reported by Bauernfeind, Widder, and Braun [$a=3.836$ Å and $c=28.58$ Å (Ref. 3)]. It is particularly interesting to note that the *a*-axis lattice parameter is within the range of that observed in $RuSr_2GdCu_2O_8$ [$a=3.838$ Å (Ref. 3)]. In the case of $RuSr_2GdCu_2O_8$ it is assumed that the rotations of the RuO_6 octahedra are driven by the large Ru-O-Ru bond length when compared with the Cu-O-Cu bond length. Thus, a similar *a*-axis lattice parameter in both $RuSr_2GdCu_2O_8$ and $RuSr_2Gd_{2-x}Ce_xCu_2O_{10+\delta}$ may indicate that $RuSr_2Gd_{2-x}Ce_xCu_2O_{10+\delta}$ also has a rotation of the RuO_6 octahedra.

We find that, while the structure of $RuSr_2Gd_{2-x}Ce_xCu_2O_{10+\delta}$ contains the electron-doped $T'R_{2-x}Ce_xO_2$ substructure, there is no evidence of the corresponding phonon modes. This is apparent in Fig. 2 where we plot the room-temperature Raman spectra from $RuSr_2Gd_{1.4}Ce_{0.6}Cu_2O_{10+\delta}$. The four peaks at ~260, ~320, ~440, and ~650 cm^{-1} are also observed in $RuSr_2GdCu_2O_8$ and have been attributed to oxygen vibrations arising from the Ru-O-Ru, Cu-O-Ru (out of phase), Cu-O-Cu (in phase), and Ru-O-Cu bonds, respectively.[14] There is no evidence in the Raman spectra for peaks that can be attributed to O(4) vibrations from the $R_{2-x}Ce_xO_2$ substructure. In the case of $Gd_{2-x}Ce_xCuO_4$, Raman peaks are observed at 347, 492, and

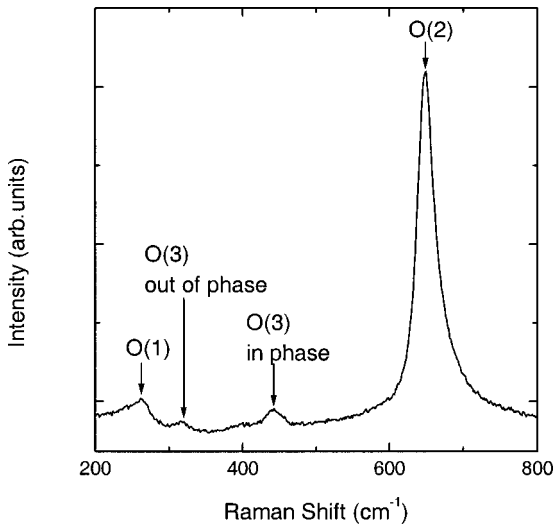

FIG. 2. Plot of the room-temperature Raman spectra from $RuSr_2Gd_{1.4}Ce_{0.6}Cu_2O_{10+\delta}$.

596 cm^{-1}. The peaks in the $Gd_{2-x}Ce_xCuO_4$ Raman spectra at 347 and 492 cm^{-1} have been attributed to B_{1g} and E_g vibrations of O(4), respectively, while the peak at 596 cm^{-1} is assigned as a A_{1g*} peak, which may be due to O(4) sites in the structures that have been rotated to be directly above Cu.[20] It can be seen in Fig. 2 that there is an additional broad peak near 400 cm^{-1} in the $RuSr_2Gd_{2-x}Ce_xCu_2O_{10+\delta}$ Raman spectra, however, this peak is not near any of the expected $R_{2-x}Ce_xO_2$ substructure peaks. The absence of O(4) vibrations in the $RuSr_2Gd_{2-x}Ce_xCu_2O_{10+\delta}$ Raman spectra may be due to disorder from a variable Ce content and a variable oxygen content in the $R_{2-x}Ce_xO_2$ substructure.

It can be seen in Fig. 3 that both the zero resistance, $T_c(0)$, and the initial decrease in the resistance, T_c, vary systematically with increasing Ce concentration. This is clearer in the inset to Fig. 3(b) where we plot $T_c(0)$ (open circles) and T_c (filled circles) against the Ce concentration. We find that $T_c(0)$ and T_c are maximum for 0.6 Ce being 35 K and 50 K for $RuSr_2Gd_{1.4}Ce_{0.6}Cu_2O_{10+\delta}$, respectively. In the case of $RuSr_2Eu_{1.4}Ce_{0.6}Cu_2O_{10+\delta}$, $T_c(0)=26$ K and $T_c=49$ K. The maximum $T_c(0)$ and T_c values are higher than those reported by Felner *et al.* [~20 and 42 K for $x=0.6$ and $R=$Gd (Ref. 1)] and are comparable to those of Bauernfield, Widder, and Braun [38 and 45 K for $x=0.5$ and $R=$Gd (Ref. 3)]. The T_c values for $RuSr_2Gd_{1.4}Ce_{0.6}Cu_2O_{10+\delta}$ are also comparable to those in $RuSr_2GdCu_2O_8$ [$T_c=45$ K (Refs. 9 and 21)]. However, T_c for $RuSr_2Eu_{1.4}Ce_{0.6}Cu_2O_{10+\delta}$ is significantly higher than that in $RuSr_2EuCu_2O_8$ [$T_c=32$ K (Refs. 16 and 21)]. It is interesting to note that the values of $T_c(0)$ and T_c in $RuSr_2Gd_{1.4}Ce_{0.6}Cu_2O_{10+\delta}$ are also significantly higher than those reported in nonmagnetic $NbSr_2Eu_{1.4}Ce_{0.6}Cu_2O_{10+\delta}$ (~13 and ~20 K, respectively[5]). This may suggest that T_c is not being significantly affected by the magnetic order in the RuO_2 layers (e.g., by possible magnetic pairbreaking).

It is apparent in Fig. 3 that the resistance data for all the as-made $RuSr_2Gd_{2-x}Ce_xCu_2O_{10+\delta}$ samples display a semiconductorlike increase for low temperatures. However, in the

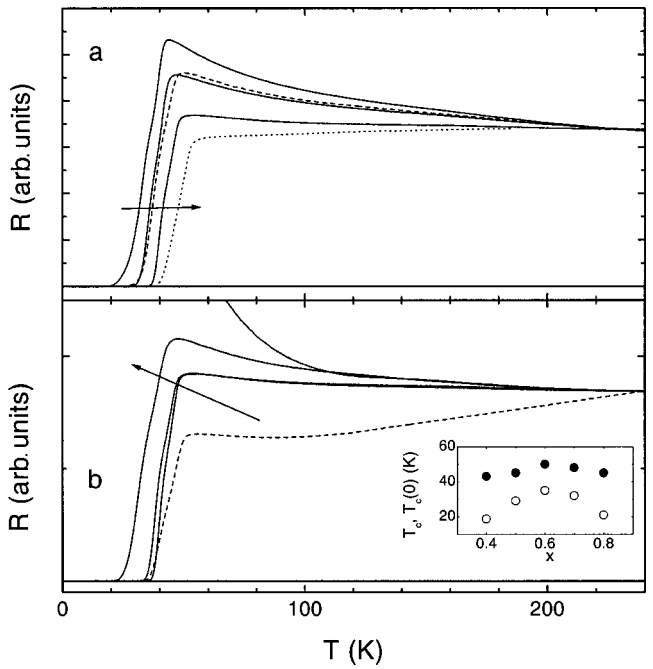

FIG. 3. Plot of the resistance from $RuSr_2Gd_{2-x}Ce_xCu_2O_{10+\delta}$ with (a) $x=0.4$, 0.5, 0.6 (b) $x=0.6$, 0.7, 0.8 1.0. The arrow indicates increasing Ce concentration. The resistance data have been vertically scaled to the same value at 220 K. Also shown is the resistance from the $RuSr_2Gd_{1.4}Ce_{0.6}Cu_2O_{10+\delta}$ sample, which was oxygen loaded at 100 bars [dotted curve, Fig. 4(a)], $RuSr_2Eu_{1.4}Ce_{0.6}Cu_2O_{10+\delta}$ [dashed curve, Fig. 4(a)], and $RuSr_2GdCu_2O_8$ [dashed curve, Fig. 4(b) (Ref. 21)]. Figure 4(b) inset: Plot of T_c and $T_c(0)$ against Ce content.

case of $RuSr_2Gd_{1.4}Ce_{0.6}Cu_2O_{10+\delta}$, which has the smallest increase, the semiconductorlike upturn disappears after oxygen loading at 100 bars as can be seen by the dotted curve in Fig. 3(a). The origin of the semiconductorlike upturn in oxygen-deficient samples is not clear. It may be partly due to oxygen depletion at the grain boundaries. We note that Bauernfeind, Widder, and Braun also observed the progressive development of a low-temperature semiconductorlike upturn with increasing oxygen deficiency.[3]

The resistance transitions are much broader than those observed in many of the other HTSC. For example, the superconducting transition width is about 14 K for the as-made $RuSr_2Gd_{2-x}Ce_xCu_2O_{10+\delta}$ sample. The superconducting transition width is broader than that observed by Bauernfeind, Widder, and Braun[3] and it is comparable to that observed by Felner *et al.*[1] Furthermore, as can be seen in Fig. 3(b), the superconducting transition width is comparable to that observed in $RuSr_2GdCu_2O_8$.[21] Part of the superconducting transition width may be due to oxygen disorder in $RuSr_2Gd_{2-x}Ce_xCu_2O_{10+\delta}$ and structural disorder in $RuSr_2GdCu_2O_8$. However, we note that a broad superconducting transition is also expected within the spontaneous vortex phase model.

Unlike some other dopants in HTSC we find that most of the additional electrons introduced by Ce do not appear to be significantly altering the hole concentration on the CuO_2 planes. This is apparent in the inset to Fig. 3(b) where it can

be seen that an increase in x from 0.4 to 0.8 results in a small increase and then decrease in T_c. If all of the electrons were doped onto the CuO_2 planes then the hole concentration n should decrease by 0.2. However, by comparison with other HTSC,[22] a decrease in n by 0.2 should result in large changes in T_c. This is apparent by noting that most HTSC have been shown to follow the $T_c(n)$ correlation, $T_c(n)=T_{c,\max}[1-82.6(n-0.16)^2]$ where superconductivity occurs for $0.05 \leqslant n \leqslant 0.27$.[22] Thus if $RuSr_2R_{2-x}Ce_xCu_2O_{10+\delta}$ is underdoped ($n<0.16$) then T_c should decrease from 43 K for $x=0.4$ to 0 for $x>0.6$, which is obviously not the case. On the other hand, if we assume that $RuSr_2Gd_{2-x}Ce_xCu_2O_{10+\delta}$ is overdoped, then by comparison with other HTSC, T_c should dramatically increase and then decrease. It is possible that, similar to $Bi_2Sr_2Ca_{1-x}Y_xCu_2O_{8+\delta}$,[23] the additional electrons introduced by Ce^{4+} are partially compensated for by an increase in δ. For example, an increase in x from 0.4 to 0.8 could be compensated for by an increase in δ of 0.2. It is also possible that the additional electrons introduced by Ce^{4+} are appearing in the RuO_2 layers. The possible effects of a change in δ or a decrease in the Ru valence can be seen using simple valence counting. In the case of $RuSr_2GdCu_2O_8$ it has been shown from a x-ray absorption near-edge spectroscopy (XANES) study that the Ru valence is +4.6.[24] Thus, from simple valence counting, this gives a Cu valence of $p=+2.2$, which is close to that of underdoped $YBa_2Cu_4O_8$ and underdoped $YBa_2Cu_3O_{7-\delta}$. From the similar T_c values of $RuSr_2R_{2-x}Ce_xCu_2O_{10+\delta}$ and $RuSr_2GdCu_2O_8$ we might expect that the Cu valence is also $\sim+2.2$ in $RuSr_2R_{2-x}Ce_xCu_2O_{10+\delta}$. Thus, using $p=0.5+\delta+(y-x)/2$, where $5-y$ is the average Ru valence, assuming that $p=+2.2$ and using $y=0$ for $x=0.5$,[25] we find that $\delta=0.03$ for $x=0.5$. It is possible that $p=+2.2$ is maintained for increasing x by a corresponding increase in δ.

We show later that there are significant changes in the low-field magnetization data commencing between 70 and 130 K, depending on the Ce concentration. If the RuO_2 layers contributed significantly to the normal-state conductivity then we might expect the magnetic ordering in the RuO_2 layers to be mirrored by a decrease in the resistance. This is observed in other ruthenate compounds.[26–28] For example, there is a decrease in the $SrRuO_3$ resistance near the ferromagnetic-ordering temperature (160 K).[26] However, it is clear in Fig. 3 that it is not observed in $RuSr_2Gd_{1.4}Ce_{0.6}Cu_2O_{10+\delta}$, even after the 100-bar anneal, and it is also not observed in $RuSr_2RCu_2O_8$.[9,12,21] In the case of $RuSr_2RCu_2O_8$ the effect of the RuO_2 layers is observed indirectly by magnetoresistance measurements.[12,21] It is therefore possible that the RuO_2 layers in $RuSr_2Gd_{1.4}Ce_{0.6}Cu_2O_{10+\delta}$ do not contribute directly to the normal-state conductivity (i.e., $\sigma_{RuO_2} \ll \sigma_{CuO_2}$).

We show in Fig. 4 that the thermopower also changes with increasing Ce concentration. It can be seen in the inset to Fig. 4(a) that the room-temperature thermopower initially decreases and then increases with increasing Ce concentration (filled circles). It had previously been argued in the case of $RuSr_2GdCu_2O_8$ that the room-temperature thermopower $S(300\,\mathrm{K})$ of $RuSr_2GdCu_2O_8(\sim 60\,\mu\mathrm{V/K})$ is indicative of a very underdoped high-temperature superconductor (HTSC) [$n\sim0.065$ (Ref. 9)]. This was based on the $S(300\,\mathrm{K})$ hole-concentration correlation,[29] which has been found for most of the HTSC's. A similar interpretation of $S(300\,\mathrm{K})$ for $RuSr_2Gd_{1.4}Ce_{0.6}Cu_2O_{10+\delta}$ would imply that $RuSr_2Gd_{2-x}Ce_xCu_2O_{10+\delta}$ is a hole-doped HTSC and the maximum hole concentration is ~0.10 for $x=0.6$. However, there is a problem because according to the $S(300\,\mathrm{K})$ vs hole-concentration correlation, $S(300\,\mathrm{K})$ for $RuSr_2Gd_{2-x}Ce_xCu_2O_{10+\delta}$ should systematically increase with increasing Ce concentration (i.e., decreasing hole concentration). It may be that like $La_{2-x}Sr_xCuO_4$,[30] $RuSr_2Gd_{2-x}Ce_xCu_2O_{10+\delta}$ does not follow the $S(300\,\mathrm{K})$ vs hole-concentration correlation or the electrons introduced by Ce^{4+} are partially compensated for by an increase in δ.

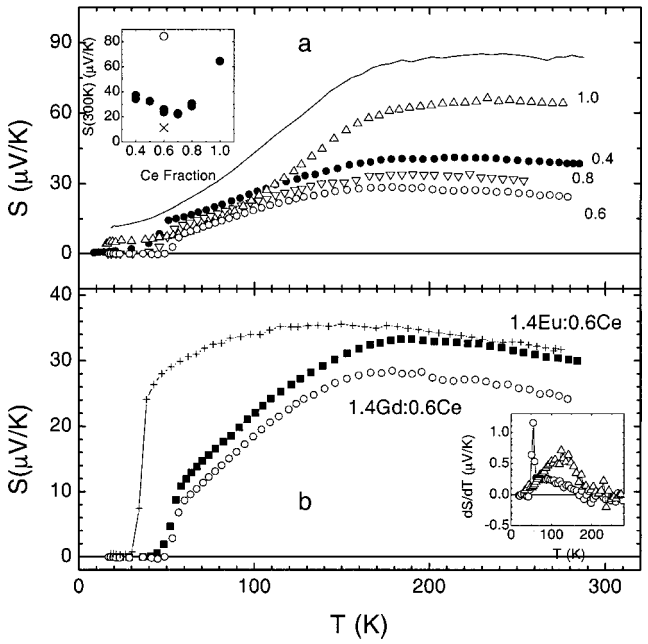

FIG. 4. (a) Plot of thermopower against temperature from $RuSr_2Gd_{2-x}Ce_xCu_2O_{10+\delta}$ with $x=1.0$ (open up triangles), 0.8 (open down triangles), 0.6 (open circles), and $x=0.4$ (filled circles). Also included is the thermopower from $RuSr_2Gd_{1.4}Ce_{0.6}Cu_2O_{10+\delta}$ that had been annealed at 600 °C in 0.1% O_2 (solid curve). Inset: Plot of $S(300\,\mathrm{K})$ against Ce fraction for as-made $RuSr_2Gd_{2-x}Ce_xCu_2O_{10+\delta}$ (filled circles) from $RuSr_2Gd_{1.4}Ce_{0.6}Cu_2O_{10+\delta}$ that had been annealed at 600 °C in $0.1\%O_2$ (open circle) and from $RuSr_2Gd_{1.4}Ce_{0.6}Cu_2O_{10+\delta}$ that had been oxygen loaded at 100 bars (cross). (b) Plot of the thermopower against temperature for $RuSr_2Gd_{1.4}Ce_{0.6}Cu_2O_{10+\delta}$ (open circles), $RuSr_2Eu_{1.4}Ce_{0.6}Cu_2O_{10+\delta}$ (filled squares), and $La_{1.87}Sr_{0.13}CuO_4$ (plus symbols). Inset: Plot of the thermopower derivative against temperature for $RuSr_2Gd_{1.4}Ce_{0.6}Cu_2O_{10+\delta}$ (open circles) and $RuSr_2GdCeCu_2O_{10+\delta}$ (open up triangles).

The effect of oxygen unloading is to increase $S(300\,\mathrm{K})$ while oxygen loading decreases $S(300\,\mathrm{K})$ as can be seen in Fig. 4(a) inset for the $RuSr_2Gd_{1.6}Ce_{0.4}Cu_2O_{10+\delta}$ sample. The decrease in oxygen content for the oxygen unloaded sample corresponds to a maximum decrease in the hole concentration in the CuO_2 planes of 0.10. It might be expected that a decrease in δ of 0.10 is equivalent to a 0.20 increase in the

Ce content. However, this does not appear to be the case because $S(300\,\mathrm{K})$ for the oxygen-reduced sample is even higher than that for the 1.0 Ce sample. We show later that changes in the magnetic order correlate with a decrease in δ of 0.10 corresponding to an increase in x of 0.20.

The temperature dependence of the thermopower for $RuSr_2R_{2-x}Ce_xCu_2O_{10+\delta}$ has features similar to those found in $RuSr_2RCu_2O_8$.[9,21] In particular, $S(T)$ is flat or initially increases with decreasing temperature. At a lower temperature of ~170 K, $S(T)$ begins to decrease for all the samples studied. This is clearer in the inset to Fig. 4(b) where we plot dS/dT against temperature for $RuSr_2Gd_{1.4}Ce_{0.6}Cu_2O_{10+\delta}$ (open circles). The normal-state temperature dependence of the derivative is essentially the same for all the superconducting $RuSr_2R_{2-x}Ce_xCu_2O_{10+\delta}$ samples and is only different for nonsuperconducting $RuSr_2RCeCu_2O_{10+\delta}$ (open up triangles). Although there is no generally accepted model for the thermopower in the HTSC, we believe that the thermopower is dominated by the CuO_2 layers. In two of the other HTSC's, which contain CuO_2 planes and conducting CuO chains or CuO ribbons, it has been shown that the thermopower can be modeled as $S(T)=(\sigma_{CuO_2}/\sigma_T)S_{CuO_2}+(\sigma_{CuO}/\sigma_T)S_{CuO}$, where σ_{CuO_2} is the conductivity from the CuO_2 planes, σ_{CuO} is the conductivity from the CuO chain or ribbons, σ_T is the total conductivity, S_{CuO_2} is the thermopower from the CuO_2 planes, and S_{CuO} is the thermopower from the CuO chain or ribbons.[30–32] Thus, the interpretation of the $RuSr_2R_{2-x}Ce_xCu_2O_{10+\delta}$ resistance data in terms of $\sigma_{RuO_2} \ll \sigma_{CuO_2}$ can lead to the thermopower being dominated by the CuO_2 layers.

It is important to note that the decrease in the thermopower below ~170 K does not imply that the decrease is somehow related to the magnetic order. This is apparent in Fig. 4(b) where we also plot the thermopower from underdoped $La_{1.87}Sr_{0.13}CuO_4$ (crosses). It can be seen that $La_{1.87}Sr_{0.13}CuO_4$ displays general features similar to those seen in $RuSr_2Gd_{2-x}Ce_xCu_2O_{10+\delta}$, except that the decrease in $S(T)$ occurs at a lower temperature (~130 K). Furthermore, as we show later, the peak in the zero-field-cooled magnetization and the saturation magnetization systematically increase with increasing Ce concentration. However, this is not reflected by changes in the temperature dependence of the thermopower.

The rapid decrease in $S(T)$ for $RuSr_2R_{2-x}Ce_xCu_2O_{10+\delta}$ at low temperatures signals the onset of superconductivity. We find that the zero-thermopower temperature (49 K for $R=$Gd and 41 K for $R=$Eu for $x=0.6$) is close to T_c as determined from the resistance data. Similar behavior is observed in $RuSr_2GdCu_2O_8$, where zero thermopower occurs at ~49 K, the resistance begins to decrease below 45 K, and a specific-heat jump is observed at 45 K.[9,21]

It is apparent in Fig. 5(a) that there are systematic changes in the low-field zero-field-cooled (ZFC) magnetization M_{ZFC} from $RuSr_2Gd_{2-x}Ce_xCu_2O_{10+\delta}$ with increasing Ce concentration. In particular, there is a peak in M_{ZFC} at a temperature T_p, which increases in temperature with increasing Ce concentration, and for higher temperatures there is a gradual decrease in M_{ZFC} with increasing temperature. Furthermore,

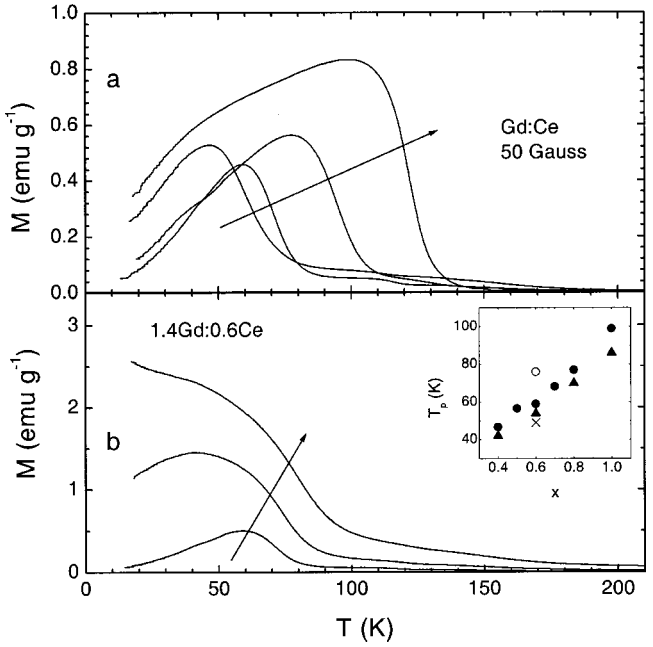

FIG. 5. (a) Plot of the zero-field-cooled magnetization at 50 G from $RuSr_2Gd_{2-x}Ce_xCu_2O_{10+\delta}$ with $x=0.4$, 0.6, 0.8, and 1.0. The arrow indicates increasing Ce fraction. (b) Plot of zero-field-cooled magnetization from $RuSr_2Gd_{1.4}Ce_{0.6}Cu_2O_{10+\delta}$ with $H=50$, 250, and 1000 G. The arrow indicates increasing H. Inset: Plot of the maximum zero-field-cooled magnetization temperature at 50 G, T_p, for $RuSr_2Gd_{2-x}Ce_xCu_2O_{10+\delta}$ (filled circles) and $RuSr_2Eu_{2-x}Ce_xCu_2O_{10+\delta}$ (filled up triangles). Also shown is T_p for the $RuSr_2Gd_{1.4}Ce_{0.6}Cu_2O_{10+\delta}$ sample annealed at 600 °C in 0.1%O_2 (open circle) and at 100 bars (cross).

this peak disappears with increasing magnetic field as can be seen in Fig. 5(b). Similar features were observed in $RuSr_2Eu_{2-x}Ce_xCu_2O_{10+\delta}$ for $x=0.5$ and $x=0.6$ where the data was interpreted in terms of localized Ru moment magnetic ordering at 180 K, slight spin canting below ~170 K, and Ru-Ru and/or Gd-Ru interactions at lower temperatures.[1,19] However, as we show later, the saturation magnetization data at 9500 G can be interpreted in terms of itinerant ferromagnetism in the RuO_2 layers. Unfortunately, there are no reports of neutron diffraction or very-high-field magnetization measurements, which would provide a better understanding of the magnetic order in $RuSr_2R_{2-x}Ce_xCu_2O_{10+\delta}$. In the absence of such data, we associate T_p with the ferromagnetic ordering in the RuO_2 layers. We note again that there was no evidence of $SrRuO_3$ (magnetic-ordering temperature of 160 K) in the XRD pattern. There was some evidence of Gd_2SrRuO_6 and Eu_2SrRuO_6 but these phases do not magnetically order above 100 K.

We show in the inset to Fig. 5(b) that T_p at 50 G increases systematically with increasing Ce concentration and there is no significant change for $R=$Gd (filled circles) or $R=$Eu (filled up triangles). It is not clear if the increase in T_p is due to the additional holes going onto the RuO_2 layers or structurally induced changes in the RuO_2 layer band structure. A similar increase in the magnetic-ordering temperature has

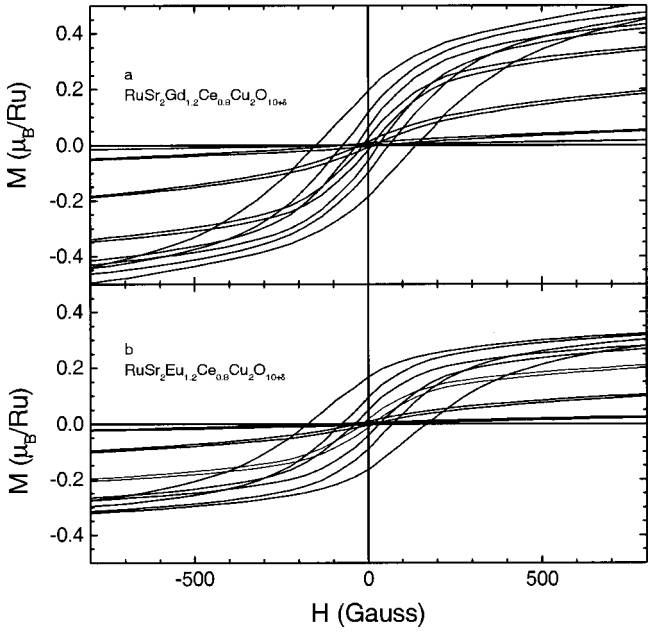

FIG. 6. Plot of the magnetization against H for (a) $RuSr_2Gd_{1.2}Ce_{0.8}Cu_2O_{10+\delta}$ with $T=17$, 37, 57, 77, 117, and 118 K; (b) $RuSr_2Eu_{1.2}Ce_{0.8}Cu_2O_{10+\delta}$ with $T=17$, 37, 56, 77, 98, and 121 K. The lower-temperature loops have larger hysteresis. The initial increase in H has been removed for clarity.

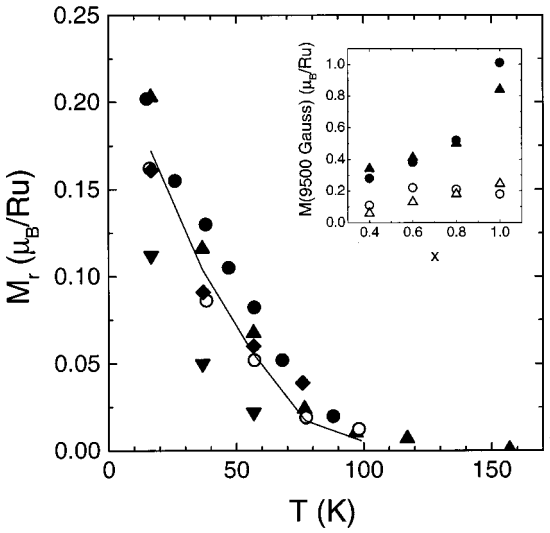

FIG. 7. Plot of the remanent magnetization against temperature for $RuSr_2Gd_{2-x}Ce_xCu_2O_{10+\delta}$ with $x=0.4$ (filled down triangles), 0.6 (filled circles), 0.8 (filled up triangles), and 1.0 (filled diamonds). Also included is the remanent magnetization from $RuSr_2Eu_{1.2}Ce_{0.8}Cu_2O_{10+\delta}$ (solid curve) and the $RuSr_2Gd_{1.4}Ce_{0.6}Cu_2O_{10+\delta}$ sample that had been annealed at 600 °C in 0.1%O_2 (open circles). Inset: Plot of the magnetization at 9500 G and 16 K from $RuSr_2Gd_{2-x}Ce_xCu_2O_{10+\delta}$ (filled circles) and $RuSr_2Eu_{2-x}Ce_xCu_2O_{10+\delta}$ (filled up triangles). The Gd^{3+} Curie-Weiss contribution was subtracted from the $RuSr_2Gd_{2-x}Ce_xCu_2O_{10+\delta}$ data. Also shown is the corresponding remanent magnetization (open symbols).

been observed in $Ca_{1-x}Sr_xRuO_3$ with increasing x for $x>0.3$.[27,33] However Ca and Sr have the same 2+ valence and hence the increase in T_p with increasing Ca concentration is not due to a simple doping effect. It is interesting to note that the removal of oxygen (i.e., the removal of holes) from $RuSr_2R_{2-x}Ce_xCu_2O_{10+\delta}$ has the same effect on T_p as an increase in Ce concentration (i.e., the removal of holes). This can be seen in the inset to Fig. 5(b) where we plot the data for the $RuSr_2R_{1.4}Ce_{0.6}Cu_2O_{10+\delta}$ sample, which had been annealed at 600 °C in 0.1%O_2 gas resulting in a decrease in δ by 0.10 (open circle) or an equivalent increase in the Ce content of 0.20. Also shown in the inset to Fig. 5(b) is T_p for the $RuSr_2R_{1.4}Ce_{0.6}Cu_2O_{10+\delta}$ sample annealed at 100 bars (cross symbol), which results in an increase in the oxygen content of 0.07. It can be seen that T_p decreases in a manner consistent with an equivalent decrease in the Ce content of 0.14.

We show in Fig. 6 that both $RuSr_2Gd_{2-x}Ce_xCu_2O_{10+\delta}$ and $RuSr_2Eu_{2-x}Ce_xCu_2O_{10+\delta}$ display similar magnetic hysteresis with increasing applied magnetic field. Here we plot the magnetization against magnetic field for $x=0.8$. The larger gradient observed for Gd is due to the large Gd moment. It can be seen that both the remanent magnetization and the coercive field decrease with increasing temperature. The resultant remanent magnetization is plotted in Fig. 7 for fully loaded $RuSr_2Gd_{2-x}Ce_xCu_2O_{10+\delta}$ (solid symbols) and $RuSr_2Eu_{1.2}Ce_{0.8}Cu_2O_{10+\delta}$ (solid curve). We find that the remanent magnetization from $RuSr_2Gd_{2-x}Ce_xCu_2O_{10+\delta}$ falls onto a common curve for $0.6\leqslant x\leqslant 1.0$ and is still finite for temperatures up to 100 K. Oxygen removal for $x=0.6$ has no significant effect on the remanent magnetization as can be seen by the open circles in Fig. 7.

We show in Fig. 8 that the magnetization saturates for moderate magnetic fields (~2500 G) after which the magnetization increases slowly with increasing magnetic field. Here we plot the magnetization from $RuSr_2Eu_{2-x}Ce_xCu_2O_{10+\delta}$ [Fig. 8(a)] and $RuSr_2Gd_{2-x}Ce_xCu_2O_{10+\delta}$ [Fig. 8(b)] at 16 K. The linear saturation of the magnetization observed in $RuSr_2R_{2-x}Ce_xCu_2O_{10+\delta}$ for magnetic fields above ~2500 G and at 16 K can be contrasted with $RuSr_2EuCu_2O_8$ [dashed curve in Fig. 8(a) and at 25 K (Ref. 16)], where the magnetization has not saturated for magnetic fields as high as 60 000 G. The magnetization for $RuSr_2Gd_{2-x}Ce_xCu_2O_{10+\delta}$ has a slope that is much greater than that of $RuSr_2Eu_{2-x}Ce_xCu_2O_{10+\delta}$, which is due to the Gd^{3+} moment. In the case of $RuSr_2Eu_{2-x}Ce_xCu_2O_{10+\delta}$, the Van Vleck paramagnetism from Eu^{3+} at 16 K is too small to account for the increase in the magnetization above ~2500 G. To characterize the saturation magnetization with increasing Ce concentration, we plot the magnetization at 9500 G and 16 K from $RuSr_2Eu_{2-x}Ce_xCu_2O_{10+\delta}$ in the inset to Fig. 7 (solid up triangles). Also plotted is the magnetization at 9500 G and 16 K from $RuSr_2Gd_{2-x}Ce_xCu_2O_{10+\delta}$ (filled circles) after subtraction of the Curie-Weiss term attributed to the Gd^{3+} moment, which is assumed to be $7\mu_B$/Gd (Ref. 2) in $RuSr_2GdCu_2O_8$. It can be seen that the saturation magnetization increases consistently for both

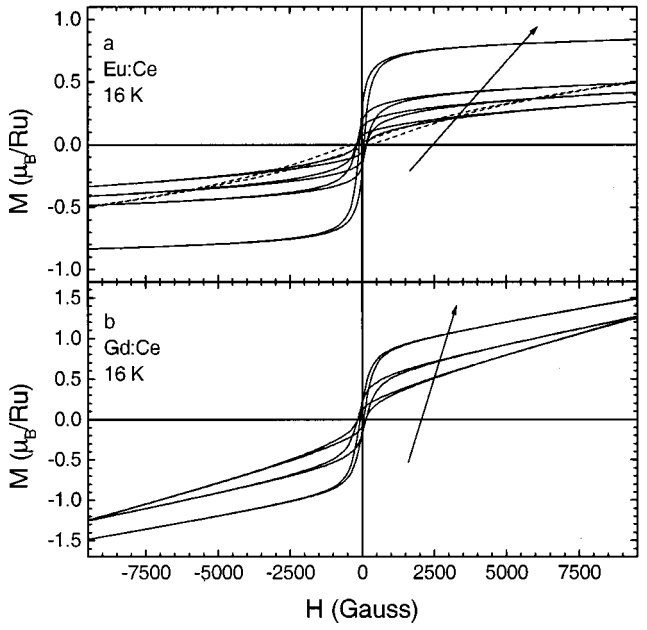

FIG. 8. (a) Plot of the magnetization against H at 16 K for $RuSr_2Eu_{2-x}Ce_xCu_2O_{10+\delta}$ with $x=0.4$, 0.6, 0.8, and 1.0. The arrow indicates increasing Ce fraction. The dashed curve is for $RuSr_2EuCu_2O_6$ and at 25 K.[16] (b) Plot of the magnetization against H at 16 K for $RuSr_2Gd_{2-x}Ce_xCu_2O_{10+\delta}$ with $x=0.6$, 0.8, and 1.0. The arrow indicates increasing Ce fraction. The initial increase in H has been removed for clarity.

$RuSr_2Eu_{2-x}Ce_xCu_2O_{10+\delta}$ and $RuSr_2Gd_{2-x}Ce_xCu_2O_{10+\delta}$. Also shown in the inset to Fig. 7 is the corresponding remanent magnetization at 16 K (open symbols).

There are a number of similarities between the magnetic and electronic behavior of the RuO_2 layers in $SrRuO_3$, $RuSr_2RCu_2O_8$, and $RuSr_2R_{2-x}Ce_xCu_2O_{10+\delta}$. For example, the octahedral crystal field results in the $4d^4$ band splitting to become a triplet (t_{2g}) state and a higher-energy doublet (e_g) valence band. Thus for Ru^{4+}, the ground state should have $S=1$ and hence the saturation moment should be $2.0\mu_B$/Ru. However, in the case of $SrRuO_3$ and $RuSr_2EuCu_2O_8$ the saturation moment at 60 kG and 5 K is only $\sim 1.3\mu_B$/Ru (Ref. 27) and $\sim 1\mu_B$/Ru (Ref. 16), respectively. Interestingly, the moment per Ru in $SrRuO_3$ has not saturated for magnetic fields as high as 300 kG [$\sim 1.4\mu_B$/Ru at 300 kG and 50 K (Ref. 27)]. In the case of $SrRuO_3$ it is now believed that $SrRuO_3$ is an itinerant ferromagnetic metal as well as a ''bad'' metal with a very small mean free path.[26,27,33] It is therefore possible that the RuO_2 layers in both $RuSr_2RCu_2O_8$ and $RuSr_2R_{2-x}Ce_xCu_2O_{10+\delta}$ display itinerant magnetic behavior. This interpretation is different from that suggested by a recent XANES study on $RuSr_2RCu_2O_8$ where the data was interpreted in terms of a mixture of Ru^{4+} and Ru^{5+} ferrimagnetism and it was suggested that there is a double-exchange interaction in the RuO_2 layers.[24] The double-exchange mechanism[34] has been invoked to explain the ferromagnetic transition in $La_{1-x}Sr_xMnO_3$, where the ordering is accompanied by a dramatic decrease in the resistivity.[35] For the double-exchange mechanism to be valid in $RuSr_2RCu_2O_8$ and $RuSr_2R_{2-x}Ce_xCu_2O_{10+\delta}$ we would expect a mixture of $t_{2g}^3e^1(Ru^{4+})$ and $t_{2g}^3(Ru^{5+})$ with $S=2$ and $S=3/2$, respectively. Therefore, we might expect the saturation magnetization to be between $4\mu_B$/Ru and $3\mu_B$/Ru. However, as mentioned above, the saturation magnetization at 9500 G and 16 K for $RuSr_2R_{2-x}Ce_xCu_2O_{10+\delta}$ is less than $1\mu_B$/Ru. Furthermore, the saturation magnetization at 60 000 G and 5 K for $RuSr_2EuCu_2O_8$ is only $\sim 1\mu_B$/Ru.

The itinerant ferromagnetic interpretation for $RuSr_2R_{2-x}Ce_xCu_2O_{10+\delta}$ conveniently explains why the saturation magnetization is less than that expected within a local moment model and why the saturation magnetization varies systematically with increasing Ce concentration. A similar increase in both the saturation magnetization and the magnetic-ordering temperature is observed in $Ca_{1-x}Sr_xRuO_2$ for $x>0.3$ where, as mentioned earlier, the substitution of Sr^{2+} for Ca^{2+} is not expected to result in a simple doping effect. The changes observed in $Ca_{1-x}Sr_xRuO_3$ have been interpreted in terms of band effects where the underlying interaction is assumed to be ferromagnetic.[26,27,33] The low-field antiferromagnetic order of $RuSr_2RCu_2O_8$ and the spin-flip transition for higher applied fields indicates that the interactions are more complex in $RuSr_2RCu_2O_8$. Antiferromagnetic order is observed in another ruthenate, Sr_2GdRuO_6, but this ruthanate is also an insulator.

CONCLUSION

We have shown that the $RuSr_2R_{2-x}Ce_xCu_2O_{10+\delta}$ transport data can be interpreted in terms of the CuO_2 layers dominating the electrical conductivity and the thermopower. There is possibly exchange coupling from the carriers in the RuO_2 layers to the conduction-band carriers in the CuO_2 layers, as is observed in $RuSr_2RCu_2O_8$. There is a low-field peak in the zero-field-cooled magnetization and the saturation magnetization increases with increasing Ce concentration. However, there is no direct correlation between these increases and the superconducting transition temperature, which may indicate that pairbreaking via coupling to the RuO_2 layers is weak. Although the temperature dependence of the magnetization is complex we show, by comparing the saturation magnetization with that from other ruthenate compounds, that the magnetic order in the RuO_2 layers can be interpreted in terms of itinerant ferromagnetism. The room-temperature Raman spectra display the same modes found in $RuSr_2RCu_2O_8$ and there is no evidence of O(4) Raman modes that are observed in the electron-doped T'HTSC. This may be due to O(4) site disorder in the $R_{2-x}Ce_xO_2$ layers, which could arise from a variable oxygen content in the $R_{2-x}Ce_xO_2$ layers.

ACKNOWLEDGMENTS

Funding support was provided by the New Zealand Marsden Fund and the Alexander von Humboldt Foundation. We acknowledge helpful discussions with H. J. Trodahl and S. Krämer. We thank R. Fairlie for oxygen loading and measuring one of the samples.

[1] A. Felner, U. Asaf, Y. Levi, and O. Milio, Phys. Rev. B **55**, 3374 (1997).
[2] C. Bernhard, J. L. Tallon, Ch. Neidermayer, Th. Blasius, A. Golnik, E. Brücher, R. K. Kremer, D. R. Noakes, C. E. Stronach, and E. J. Ansaldo, Phys. Rev. B **59**, 14 099 (1999).
[3] L. Bauernfeind, W. Widder, and H. F. Braun, Physica C **254**, 151 (1995).
[4] L. Bauernfeind, W. Widder, and H. F. Braun, J. Low Temp. Phys. **105**, 1605 (1996).
[5] L. Rukang, Z. Yingjie, Q. Yitai, and L. Zuyao, Physica C **176**, 19 (1991).
[6] T. J. Goodwin, H. B. Radousky, and R. N. Shelton, Physica C **204**, 212 (1992).
[7] J. Tallon, C. Bernhard, M. Bowden, P. Gilberd, T. Stoto, and D. Pringle, IEEE Trans. Appl. Supercond. **9**, 1051 (1999).
[8] A. C. McLaughlin, W. Zhou, J. P. Attfield, A. N. Fitch, and J. L. Tallon, Phys. Rev. B **60**, 7512 (1999).
[9] J. L. Tallon, J. W. Loram, G. W. M. Williams, and C. Bernhard, Phys. Rev. B **61**, 6471 (2000).
[10] W. E. Picket, R. Weht, and A. B. Shick, Phys. Rev. Lett. **83**, 3713 (1999).
[11] O. Chmaissem, J. D. Jorgensen, H. Shaked, P. Dollar, and J. L. Tallon, Phys. Rev. B **61**, 6401 (2000).
[12] J. E. McCrone, J. R. Cooper, and J. L. Tallon, J. Low Temp. Phys. **117**, 1199 (1999).
[13] A. Fainstein, E. Winkler, A. Butera, and J. L. Tallon, Phys. Rev. B **60**, 12 597 (1999).
[14] A. Fainstein, P. Etchegoin, H. J. Trodahl, and J. L. Tallon, Phys. Rev. B **61**, 15 468 (2000).
[15] J. W. Lynn, B. Keimer, C. Ulrich, C. Bernhard, and J. L. Tallon, Phys. Rev. B **61**, 14 964 (2000).
[16] G. V. M. Williams and S. Krämer, Phys. Rev. B **62**, 4132 (2000).
[17] A. C. McLaughlin and J. P. Attfield, Phys. Rev. B **60**, 14 605 (1999).
[18] I. Felner, U. Asaf, Y. Levi, and O. Millo, Physica C **334**, 141 (2000).
[19] E. B. Sonin and I. Felner, Phys. Rev. B **57**, 14 000 (1998).
[20] R. T. Heyen, R. Liu, M. Cardona, S. Piñol, R. J. Melville, D. McK. Paul, E. Morán, and M. A. Alario-Franco, Phys. Rev. B **43**, 2857 (1991).
[21] M. Pozêk, A. Dulĉić, D. Paar, G. V. M. Williams, and S. Krämer, Phys. Rev. B (to be published).
[22] M. R. Presland, J. L. Tallon, R. G. Buckley, R. S. Liu, and N. E. Flower, Physica C **176**, 95 (1991).
[23] G. V. M. Williams, D. M. Pooke, D. J. Pringle, H. J. Trodahl, J. L. Tallon, J. Quilty, N. Malde, J. Driscoll, A. Crossley, and L. Cohen, Phys. Rev. B **62**, 1379 (2000).
[24] R. S. Liu, L.-Y. Jang, H.-H. Hung, and J. L. Tallon, Phys. Rev. B **63**, 212507 (2001).
[25] I. Felner, U. Asaf, C. Godart, and E. Alleno, Physica B **259–261**, 703 (1999).
[26] P. B. Allen, H. Berger, O. Chauvet, L. Forro, T. Jarlborg, A. Junod, B. Revaz, and G. Santi, Phys. Rev. B **53**, 4393 (1996).
[27] G. Cao, S. McCall, M. Shepard, J. E. Crow, and R. P. Guertin, Phys. Rev. B **56**, 321 (1997).
[28] G. Cao, S. McCall, J. E. Crow, and R. P. Guertin, Phys. Rev. Lett. **78**, 1751 (1997).
[29] S. D. Obertelli, J. R. Cooper, and J. L. Tallon, Phys. Rev. B **46**, 14 928 (1992).
[30] M. V. Elizarova and V. E. Gasumyants, Phys. Rev. B **62**, 5989 (2000).
[31] G. V. M. Williams, M. Staines, and R. H. Meinhold, Physica C **258**, 273 (1996).
[32] C. Bernhard and J. L. Tallon, Phys. Rev. B **54**, 10 201 (1996).
[33] K. Yoshimura, T. Imai, T. Kiyama, K. R. Thurber, A. W. Hunt, and K. Kosuge, Phys. Rev. Lett. **83**, 4397 (1999).
[34] J. B. Goodenough, Phys. Rev. **100**, 564 (1955).
[35] H. Asano, J. Hayakawa, and M. Matsui, Phys. Rev. B **56**, 5395 (1997).